ELSEVIER

Chemical Geology 172 (2000) 95–112

CHEMICAL GEOLOGY
INCLUDING
ISOTOPE GEOSCIENCE

www.elsevier.com/locate/chemgeo

Low temperature replacement of monazite in the Ireteba granite, Southern Nevada: geochronological implications

K.J. Townsend [a], C.F. Miller [a,*], J.L. D'Andrea [a,b], J.C. Ayers [a], T.M. Harrison [b], C.D. Coath [b]

[a] *Geology Department, Vanderbilt University, Nashville, TN 37235, USA*
[b] *Department of Earth and Space Sciences, UCLA, Los Angeles, CA 90024, USA*

Abstract

The Ireteba pluton is a relatively homogeneous, ~64 Ma (zircon ion probe age) two-mica granite that was intruded by two 16 Ma Miocene plutons at depths ranging from 5 to 13 km. Deeper levels of the Ireteba and Miocene plutons were ductilely deformed at 15–16 Ma. At shallow levels remote from the Miocene plutons, the Ireteba granite appears to have experienced little Miocene heating and deformation.

Monazites from different portions of the pluton reflect the different histories experienced by the host rock. Irregularly shaped (patchy) zones with high huttonite component ($ThSiO_4$) are widespread in monazite at deep levels adjacent to Miocene plutons but less common in shallow-level rock; monazite grains with extensive replacement generally have irregular, embayed surfaces. In undeformed rocks distant from the Miocene plutons, monazites are less modified and more nearly euhedral, though fine networks of replacement veins are common and irregular rims are evident in some grains. Secondary monazite from these samples is poorer in huttonite. Ion probe Th–Pb dating yields 60–65 Ma ages for magmatic and some replacement zones in monazite from the shallow samples, and veins yield apparent ages as young as mid-Tertiary. Monazites from deep samples yield a few 55–65 Ma ages for remnant magmatic zones and abundant Miocene ages for replacement zones (~14–18 Ma). These data demonstrate extensive Miocene replacement of magmatic monazite, especially at deep levels near Miocene plutons, and they suggest an early replacement episode as well. Both events were probably related to influxes of fluid; the first may have been associated with initial solidification of the Ireteba pluton and the second with the Miocene plutons and/or extensional deformation. Ambient temperatures at the time of replacement indicate that secondary monazite growth occurred at T as low as 400°C or less.

Keywords: Monazite; U–Th–Pb geochronology; Replacement; Granite

1. Introduction

Monazite is a light rare earth element (LREE) phosphate mineral that contains high concentrations of the radioactive elements U and Th and incorporates little common Pb into its crystal structure. It commonly occurs as an accessory phase in peraluminous granites and in metamorphosed quartzofeldspathic and aluminous rocks of amphibolite and granulite facies. Natural and experimental studies demonstrate that monazite retains Pb up to relatively high temperatures and suggest a typical closure tem-

* Corresponding author. Tel.: +1-615-322-2976; fax: +1-615-322-2138.
E-mail address: millercf@ctrvax.vanderbilt.edu (C.F. Miller).

0009-2541/00/$ - see front matter
PII: S0009-2541(00)00238-2

perature of about 700–750°C (Copeland et al., 1988; Heaman and Parrish, 1991; Suzuki et al., 1994; Smith and Giletti, 1997). These qualities make monazite a preferred mineral for dating by U–Th–Pb methods, particularly in circumstances where inheritance in zircon is substantial (Hawkins and Bowring, 1997).

Monazite has been used extensively over the past decade to determine ages of magmatic crystallization and of prograde and peak metamorphism in metamorphic rocks (e.g. Parrish, 1990; Smith and Barreiro, 1990; Kingsbury et al., 1993). Such studies generally assume that the monazite is a closed system below its Pb closure temperature. Recent studies show, however, that this assumption is not always valid and suggest that monazite geochronology is complex. These studies show that secondary modification of monazite, as indicated by irregular zoning, may be widespread (DeWolf et al., 1993; Poitrasson et al., 1996; Fitzsimmons et al., 1997; Hawkins and Bowring, 1997, 1999; Miller et al., 1997; Zhu et al., 1997; Crowley and Ghent, 1999; Vavra and Schaltegger, 1999). Recrystallization or replacement of discrete zones should result in complete resetting of the U–Th–Pb system within these zones, and hence more complex, but potentially more instructive, radiometric data, given that not all grains were entirely recrystallized (DeWolf et al., 1993; Hawkins and Bowring, 1997).

Conventional U–Th–Pb dating of monazite involves dissolution of entire monazite grains or grain populations, or more recently fragments of grains, and measurement of U–Th–Pb ratios by thermal ionization mass spectrometry (e.g. Parrish, 1990; Hawkins and Bowring, 1997). Concordant monazite U–Pb ages are common in such analyses, though sometimes requiring correction for thorogenic ^{206}Pb (Schärer, 1984), and are often accepted as the best estimate of the age of magmatic crystallization or prograde to peak metamorphism (e.g. Parrish, 1990; Smith and Barreiro, 1990; Kingsbury et al., 1993; Harrison et al., 1995; cf. Hawkins and Bowring, 1997). If replacement of primary monazite is common, and especially if replacement zones are distributed throughout grains, then such interpretations must be viewed with caution. This is particularly important where replacement zones are Th-rich and therefore may strongly influence the apparent age of whole grains. If replacement occurred within a few tens of millions of years of original crystallization, discordance resulting from partial replacement would not be evident in U–Th–Pb dates because they would still overlap concordia within their uncertainties; this may result in erroneous age interpretations.

In situ, high mass resolution ion microprobe (IMP) analysis has become available more recently to obtain U–Th–Pb ages on spots as small as ~ 10 μm in diameter (Kroener and Williams, 1993; Harrison et al., 1995). IMP analysis is capable of dating multiple events recorded in a single grain, but it may also yield spurious dates if analysis spots overlap multiple zones. This problem can be minimized by using backscattered electron (BSE) imaging to guide selection of IMP spots in specific zones (Hanchar and Miller, 1993). The presence of multiple growth zones interferes with simple thermochronological interpretation, but it provides an opportunity for acquiring additional information about the nature and timing of replacement events that may be of considerable geologic significance. Recognizing and understanding events that cause monazite replacement is therefore important, both in avoiding misinterpretation and potentially in taking advantage of the ability to date additional tectonically significant rock-modifying processes.

Monazite and zircon were initially separated from samples of granite from the Ireteba pluton and the nearby White Rock Wash pluton of the Eldorado and Newberry Mountains, southern Nevada (Miller et al., 1997; D'Andrea, 1998). Our aim was to date the plutons and search for inheritance, but during that investigation, we observed what appeared to be secondary zones within the grains. Our samples for the initial study provided a preliminary comparison of monazite's response to the different conditions that affected various parts of the pluton. We noted that replacement was extensive in structurally deep rocks that underwent ductile deformation, whereas rocks that were farther removed from the effects of Miocene plutons and later deformation contained monazite that appeared to be less modified. These observations encouraged us to study the effects of variable post-crystallization histories on monazite from the Ireteba granite.

The objectives of this study are to (1) present textural, age, and chemical data for Ireteba mon-

azites; (2) discern patterns in these data as they relate to temperature, depth, deformation, and proximity to younger plutons; (3) evaluate possible causes of replacement in monazite; and (4) determine the number and age of replacement episodes that affected Ireteba monazites.

2. Geologic setting

The Ireteba granite, located in the Eldorado Mountains, southern Nevada (Fig. 1), is a two-mica granite composed of plagioclase and potassium feldspars, quartz, biotite, muscovite, and accessory minerals (D'Andrea, 1998). It is relatively homogeneous geochemically and mineralogically but varies in post-crystallization history. Zircon IMP dating indicates an age of 64 ± 2 Ma (D'Andrea, 1998; D'Andrea and Miller, unpublished data). The overall history of this granite is relatively well known, and thus there are constraints on the timing and conditions of monazite growth.

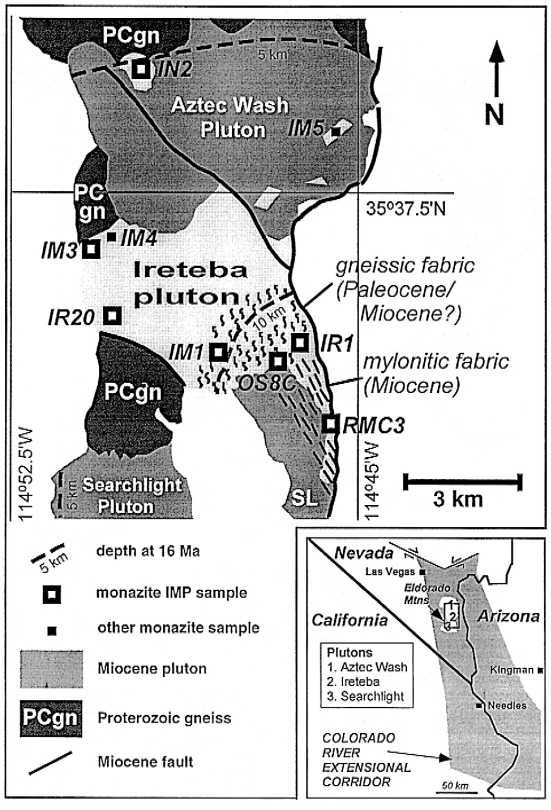

Fig. 1. Sketch map of the Ireteba pluton with sample locations, distribution of deformational fabric, and surrounding rock types. Depths at 16 Ma based on hornblende barometry for Miocene plutons (Patrick and Miller, 1997; Bachl, 1997).

The Eldorado Mountains are in the northern part of the Colorado River Extensional Corridor, a region that experienced major extensional activity and magmatism between 16 and 11 Ma. Peak extension and plutonism occurred at 15–16 Ma (Faulds et al., 1990; Gans and Landau, 1993; Falkner et al., 1995; Bachl, 1997). Extensional faulting tilted the pluton so that deeper levels are exposed toward the southeast, making it possible to study a cross-sectional profile. Hornblende barometry for the 15.7 ± 0.2 Ma Aztec Wash and 16.5 ± 0.3 Ma Searchlight plutons, both of which intruded the Ireteba pluton, documents Miocene tilting to the west and northwest (Falkner et al., 1995; Bachl, 1997; Patrick and Miller, 1997). The northern Aztec Wash pluton solidified at ~ 5 km and the southern end (bottom) of the pluton solidified at ~ 7.5 km. The Searchlight pluton was emplaced at depths ranging from ~ 3 km in the west to 13 km in the east. Thus, the intervening Ireteba pluton was at depths of ~ 5 to 13 km at 16 Ma.

Fabrics that vary throughout the Ireteba pluton document the effects of a Miocene episode and possibly a late Cretaceous–early Paleocene episode of ductile deformation in deep parts of the pluton (cf. Shaw et al., 1995; Bachl, 1997), whereas shallower parts have undergone only modest brittle deformation. Much of the pluton appears to be unaltered, but the large, adjacent 16 Ma plutons to the north and south (Falkner et al., 1995; Bachl, 1997) reheated, diked, and caused minor local hydrothermal alteration in the Ireteba pluton, especially in the deeper southeastern parts. Ductile deformation resulted in a west-dipping, largely planar fabric shared by the Searchlight pluton to the south and a strong west-plunging linear fabric that may be related to Late Cretaceous–Paleocene deformation (cf. Carl et al., 1991) or, more likely, to Miocene extension in the Colorado River Extensional Corridor. Ductile fabric is restricted to the deeper southeastern part of the pluton.

3. Methods

Two to seven kilogram samples from nine locations in the Ireteba pluton were selected to represent the textural variation in the pluton and to transect it from top to bottom (before tilting). Samples were collected from the following: (1) the most pristine rock available (no apparent alteration or deformational fabric); (2) a xenolith in a Miocene pluton; (3 and 4) contacts with Miocene plutons at shallow and deep levels; (5 and 6) ductilely deformed rock with strongly linear and planar fabrics; (7) deep-level rock with a weak, high-temperature fabric; and (8) pegmatite associated with Ireteba granite.

Monazite was separated by standard methods, handpicked, mounted in epoxy along with UCLA standard 554, polished, and coated first with carbon (for scanning electron microscopy (SEM) and EMP work), then with gold (for IMP work). Internal structures of the epoxy-mounted grains were "mapped" by BSE imaging. Most grains were mapped using the JEOL 733 Superprobe at Rensselaer Polytechnic Institute, and some were mapped with the Hitachi S-4200 SEM at Vanderbilt University. Variations in BSE brightness, which correlates with mean atomic number, reveal micron-scale compositional variation. Huttonite ($ThSiO_4$) content is thought to be the principal control of BSE brightness because the huttonite substitution results in a considerably higher atomic number and our analyses show that huttonite content correlates well with brightness. Surface textures of a few representative grains from three samples were inspected on the Hitachi SEM at Vanderbilt. Elemental analyses of monazite were performed using the JEOL 733 Superprobe at Rensselaer Polytechnic Institute following the procedures of Wark and Miller (1993).

Grains were viewed on the Cameca ims 1270 high-resolution IMP at UCLA by reflected light, and thus it was necessary to match the shape and crack geometry of grains with the BSE images to locate analysis spots. IMP techniques followed those described in Harrison et al. (1995). Most analyses employed a 15×20 μm spot. Th–Pb ages are presented on summed probability plots (Fig. 5), that is, as the sum of Gaussian distributions for individual analyses based on their analytical uncertainties (Deino and Potts, 1992).

4. Results

4.1. Surface textures

Surfaces and external morphology of monazite grains, observed during handpicking and reconnaissance SEM study, ranged from euhedral with well developed faces to highly irregular and pitted (Fig. 2). Euhedral crystals are rare or absent in most

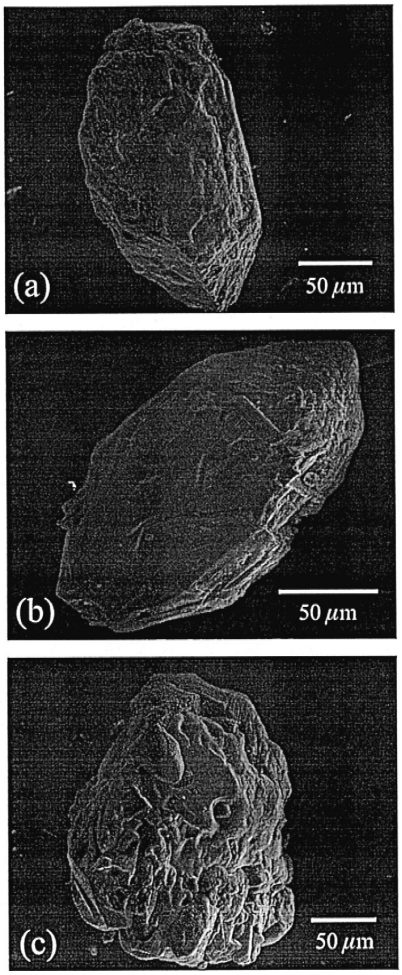

Fig. 2. SEM images of monazite grains illustrating typical surface textures. (a) Sample IM3 (note euhedral shape with moderate surface pitting); (b) sample IM1 (note euhedral shape with minor surface pitting); and (c) sample OS8C (note anhedral shape, heavily pitted surface). Monazites from samples IM3 and IM1 have limited internal replacement, whereas OS8C monazites are very extensively replaced.

samples, and extent of pitting correlates crudely with development of complex internal zoning (see below).

4.2. Internal zoning textures

Zoning textures observed by BSE imaging formed the primary basis for paragenetic interpretation and guided EMP and IMP analysis. Textures were subdivided into seven categories based on their geometry:

1. *euhedral*, commonly oscillatory zoning (Fig. 3a,b,h);
2. *veins*, occurring in two varieties: fine and abundant (~1 μm), and thick and sparse (~8–10 μm), both of which are always brighter in BSE image than the surrounding grain, which is either homogeneous or oscillatory zoned (Fig. 3b,c,d);
3. irregular, discontinuous *rims* (Fig. 3d);
4. *patchy* zoning, fairly large (tens of microns) areas with variable, ameboid shapes, and sharp boundaries; includes areas of both bright and dark BSE brightness (Fig. 3e);
5. *convolute* zoning, with sub-parallel to ribbon-like domains that may be very bright in BSE image (Fig. 3f,g);
6. *sector* zoning, consisting of angular areas of differing BSE brightness superimposed on more faintly visible oscillatory zoning (Fig. 3h); and
7. irregular *cores*, which are rare and occur in grains whose oscillatory zoning appears otherwise undisturbed.

Oscillatory (euhedral) zoning is interpreted to be magmatic and veins and patchy zones that crosscut oscillatory zoning to represent replacement. In general, the most intense replacement of magmatic zoning is present in monazite that is anhedral and has grain surface textures that are pitted and irregular (Fig. 2).

Table 1 describes the distribution of monazite zoning textures in the pluton. Oscillatory zoning is present in monazite from all samples. In some grains, oscillatory zoning is undisturbed, whereas in others, it occurs with veins, patchy zones, irregular rims or recrystallized cores. Veins are almost entirely restricted to monazite from shallow samples, and they are completely absent at the deep contact zone with the Searchlight pluton. The majority of veined grains, particularly those with fine veins, are otherwise largely unzoned. A few oscillatory-zoned grains have relatively thick veins. Patchy zones are found in all samples and in association with all other types of zoning, with the degree of patchiness generally increasing with depth. Irregular rims are present on some veined and patchy grains. Convolute zoning is found only in the deep sample at the contact with the Searchlight pluton (sample OS8C), where it is associated with extremely patchy zoning. Recrystallized cores are present in a few grains from sample IM1, which is deformed but not in a contact zone with Miocene plutons. Several patchy grains from sample IR1 (deep in the pluton) display a fine, discontinuous ring of bright BSE spots close and roughly parallel to the grain surface; most of these grains also show remnants of oscillatory zoning.

It appears that the volume of the interior of the crystal does not change upon recrystallization, that is, replacement is roughly volume-for-volume. All types of replacement zoning eliminated primary zoning in the affected area without disturbing oscillatory bands in adjacent parts of the grain, and crosscutting veins do not offset oscillatory zoning. There is, however, clear evidence for at least some volume loss at the surface (irregular shapes, truncation of euhedral zones at the surfaces) and in some cases, possible development of secondary overgrowths (thick, irregular rims) (Figs. 2, 3).

4.3. Geochronology

Most oscillatory zones yield IMP ages between 59 and 65 Ma. Patchy zones range from 14 to 67 Ma, but these fall mainly into two groups: 60–64 and 14–18 Ma. Irregular rims large enough to be dated yield ages from 56 to 67 Ma, with no Miocene ages. Convolute zones, all from the deep contact zone sample, were between 14 and 15 Ma. Unfortunately, IMP optics make precise locating of spots, difficult and therefore none of the analyses of thin replacement veins were exclusively of vein material. Apparent vein "ages" ranged from 22 to 46 Ma, but given that IMP spots overlapping larger portions of vein material yielded younger ages, we suspect the veins are Miocene.

Fig. 4 is a probability plot of the IMP ages. The curve shows two frequency spikes, the first being

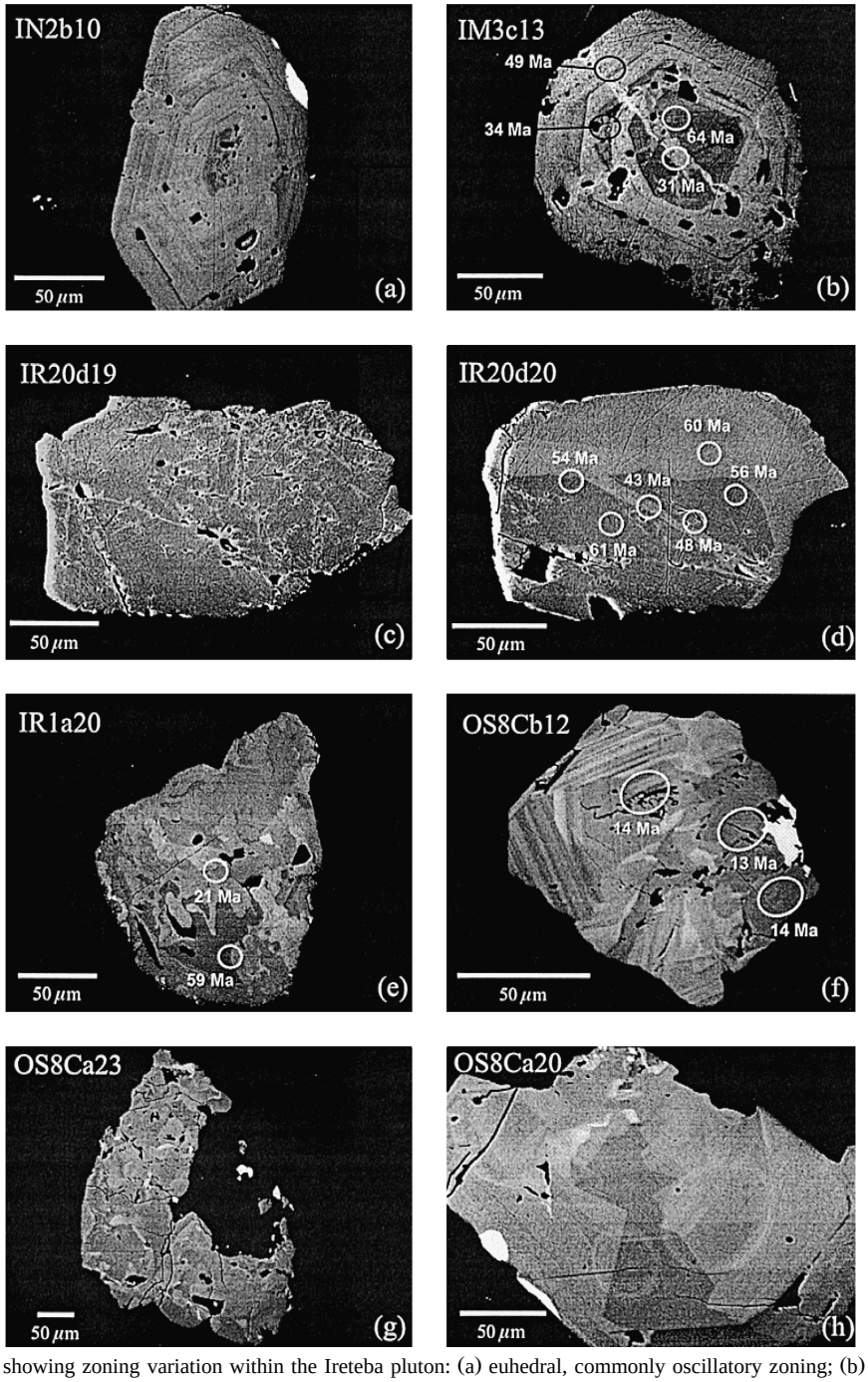

Fig. 3. BSE images showing zoning variation within the Ireteba pluton: (a) euhedral, commonly oscillatory zoning; (b) thick, sparse veins (also d); (c) fine, abundant veins; (d) irregular rim; (e) patchy zoning; (f, g) convolute zoning; and (h) sector zoning (pale, light circles are artifacts of charging due to faulty carbon coat). Brightness is controlled by mean atomic number and correlates with huttonite content. See text for discussion.

Table 1
Sample environment, fabric, and monazite zoning

Sample	Fabric	Location and depth	Monazite texture
IR20	Undeformed	W, shallow	Oscillatory and weakly developed patchy zoning; fine veins are abundant; thick veins present in some grains; irregular rims up to 50 μm thick
IN2	Undeformed	NW, very shallow, small pendant of Ireteba at root of Aztec Wash pluton	Most grains oscillatory zoned; few weakly developed patchy; small veins are common; few grains show a fine ring of bright material toward the outside of the grain
IM3	Undeformed	W, shallow	Oscillatory and weakly developed patchy zoning; fine veins are abundant; thick veins present in some grains
IM1	Gneissic (low-T)	S, moderate depth	Oscillatory and patchy zoning; irregular rims up to 50 μm thick; several grains show odd cores that may be crystallized; minor veins
RMC3	Mylonitic	SE, sheared band underlying Searchlight pluton	Oscillatory and patchy zoning; grains contain many large, possibly intergrown inclusions
IM5	Undeformed	E, from ~3 m xenolith of Ireteba within Aztec Wash pluton	Patchy (one grain only)
IR1	Gneissic (high-T)	SE, deep	Oscillatory and well-developed patchy zoning; many grains display a fine ring of bright material toward the outside of the grain
OS8C	Contact	SE, deep, ~2 m from contact with Searchlight pluton	Oscillatory, convolute, sector, and well-developed patchy zoning; no veins; some grains exhibit very bright zones
IM4P	Pegmatite	W, shallow	Oscillatory and weakly to well-developed patchy zoning; irregular rims; minor veins

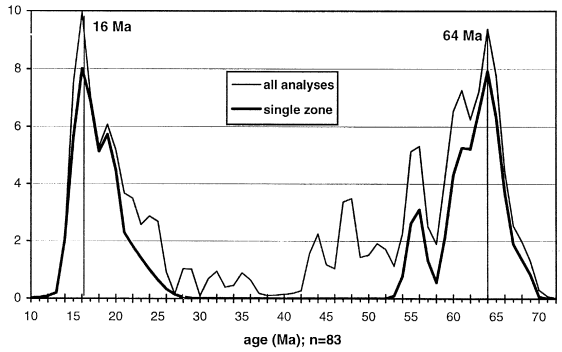

Fig. 4. Summed age probability plot for IMP Th–Pb data for all monazites. Bold line indicates age probability curve using only analyses that fell within a single zone.

around 64 Ma, the age of the pluton according to zircon IMP analysis. The second spike is around 16 Ma, which is the approximate age of the Aztec Wash and Searchlight plutons and of the most rapid extensional deformation in the area. Ages comprising the older age spike range from 59 to 69 Ma, and the younger ages are between 14 and 18 Ma. The bold curve, which excludes IMP spots that appeared to overlap multiple texture zones (determined by post-IMP SEM imaging), eliminates many dates that lie between the two major peaks. We infer that the few remaining intermediate "ages" also overlap undetected zone boundaries or reflect minor diffusive Pb loss, and thus, the true ages of monazite growth are ~16 and ~60–64 Ma.

There is a striking difference in age probability plots between samples from deep in the pluton and all others (Fig. 5); deep samples have the largest age spikes in the Miocene (14–18 Ma), while shallower samples, regardless of proximity to the Miocene

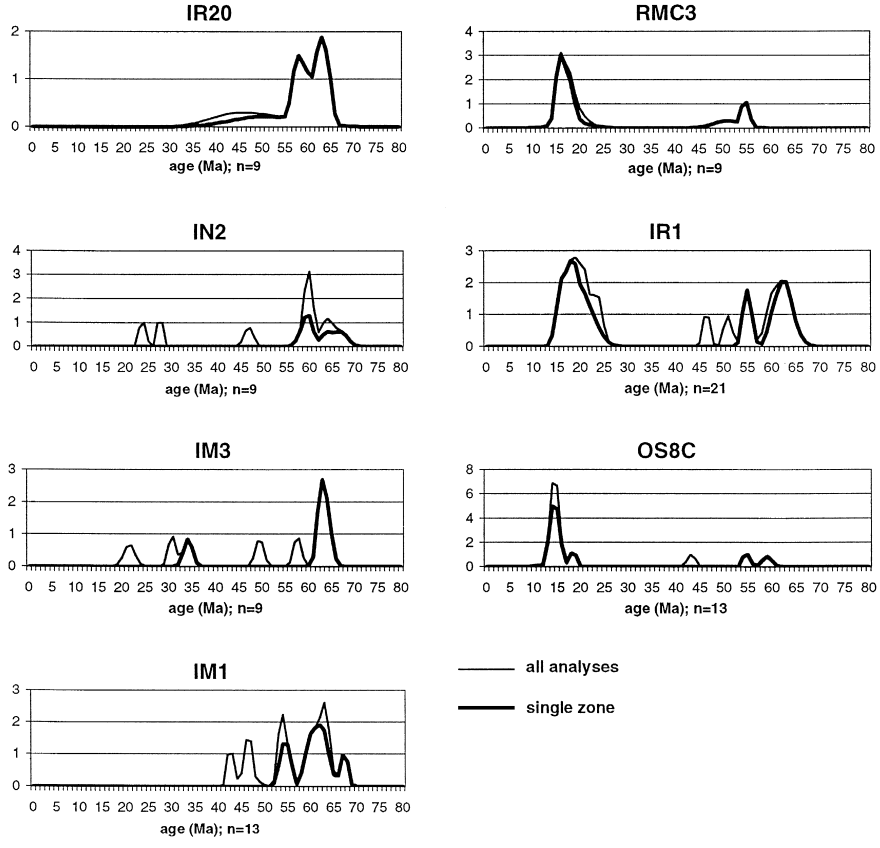

Fig. 5. Age probability plots for monazites from individual samples. Bold line indicates curve for single-zone analyses only.

Aztec Wash pluton, have the strongest spikes during the Paleocene (60–64 Ma). Deep samples RMC3, IR1, and OS8C give some Cretaceous–Paleocene ages, indicating that resetting was not complete in all grains. The resetting in these samples mostly occurred in replacement zones, though some diffusive Pb loss from primary zones may be indicated by ages younger than 60 Ma. Shallow samples IR20, IN2, IM3, and IM1 have predominantly 60–64 Ma ages but also include intermediate ages, most of which come from spots that overlapped replacement and magmatic zones. Sample IM1 is from a strongly lineated rock at intermediate depth that gives few young ages.

4.4. Compositional zoning

Monazite is primarily a solid solution among three end-members: pure REE monazite (LREE PO_4), brabantite ($CaTh(PO_4)_2$), and huttonite ($ThSiO_4$) and its U-rich equivalent ($USiO_4$). Almost all variations in monazite composition can be explained by the following substitutions (Zhu and O'Nions, 1999):

$$Th^{4+} + Ca^{2+} \rightarrow 2LREE^{3+}$$

$$U^{4+} + Ca^{2+} \rightarrow 2LREE^{3+}$$

$$Th^{4+} + Si^{4+} \rightarrow LREE^{3+} + P^{5+}$$

$$U^{4+} + Si^{4+} \rightarrow LREE^{3+} + P^{5+}.$$

Atomic abundance of Th + U in monazite should be equal to that of Ca + Si if coupled substitution is the primary mechanism for compositional change. We cannot test this fully because U concentration was not determined, but given that U is low compared to Th, Th abundance should be close to Ca + Si. Th/(Ca + Si) is close to one, particularly for replacement zones (Fig. 6a). The typical displacement of analyses toward Th/(Ca + Si) slightly less than one may reflect the presence of appreciable U. Some analyses (mainly of magmatic zones) display a distinct excess of Ca + Si, primarily because of high

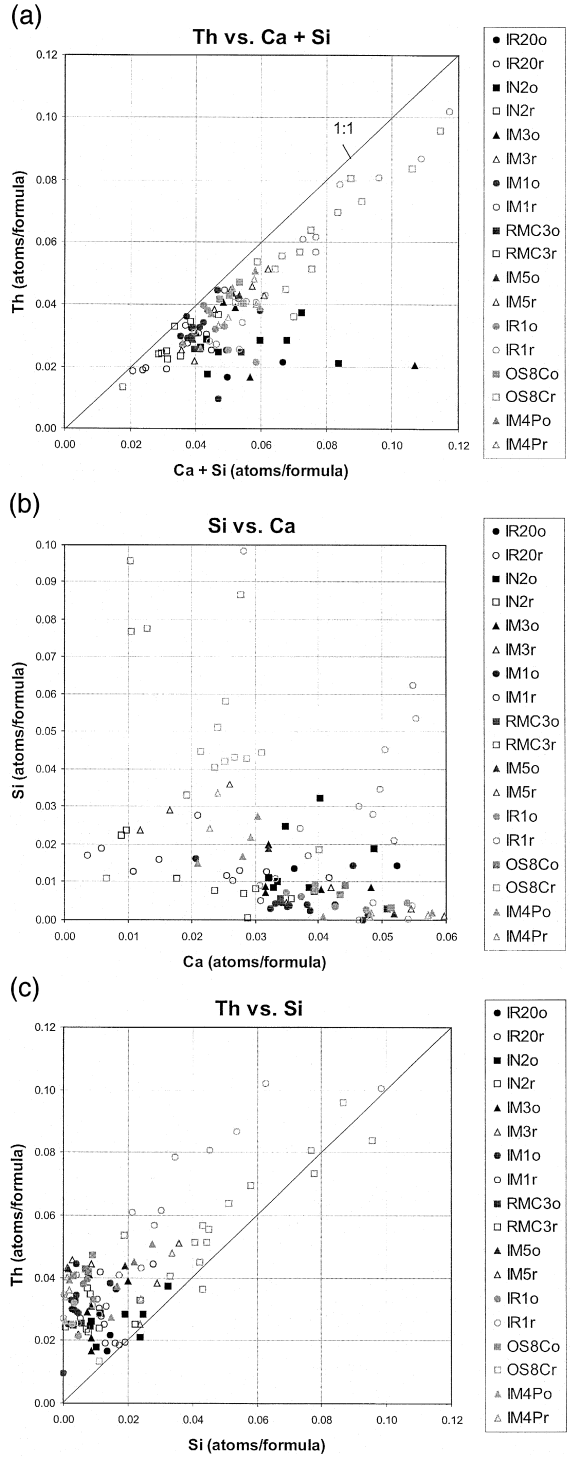

Fig. 6. (a,b) Concentrations of selected cations per formula (four oxygens per formula). Analyses of original magmatic (o; filled symbols) and replacement (r; open symbols) zones, broken down by sample.

Table 2
Average elemental composition of primary and replacement monazite zones, by sample (EMP). All compositions in oxide wt.% (AW: Aztec Wash pluton).

		Nd + Sm + Dy + Y	La + Ce	REE	La_2O_3	Ce_2O_3	Pr_2O_3	Nd_2O_3	Sm_2O_3	Dy_2O_3	Y_2O_3	ThO_2	SiO_2	CaO	P_2O_5	Total
Primary zones																
IR20	Shallow	13.1	49.2	65.2	16.9	32.3	2.8	10.7	1.2	0.28	0.90	2.7	0.27	0.98	30.2	99.3
IN2	Very shallow	13.2	48.8	65.0	16.6	32.3	3.0	11.0	1.3	0.24	0.68	3.0	0.44	0.96	30.0	99.4
IM3	Shallow	13.2	48.2	64.4	16.3	31.9	2.9	10.7	1.3	0.31	0.93	3.3	0.26	1.12	30.3	99.5
IM4P	Shallow-pegmatite	18.2	41.4	62.8	12.2	29.3	3.3	12.3	2.9	0.82	2.15	4.3	0.36	0.84	31.1	99.8
IM1	Medium-deformed	15.1	46.6	64.7	15.3	31.3	3.0	11.1	1.7	0.57	1.68	3.5	0.13	0.91	30.6	99.9
RMC3	Deep?	16.7	44.4	64.0	14.7	29.7	2.9	11.4	1.7	0.80	2.70	2.8	0.11	1.02	30.4	98.3
IM5	Xenolith in AW	17.0	42.3	62.3	13.1	29.2	3.1	11.6	2.5	0.77	2.15	4.9	0.26	1.01	30.7	99.5
IR1	Deep	15.4	45.1	63.5	14.9	30.2	3.0	11.6	1.7	0.51	1.54	3.6	0.14	1.03	30.8	99.7
OS8C	Deep	15.1	43.7	61.7	14.2	29.5	2.9	10.8	1.9	0.57	1.81	5.8	0.61	0.91	30.2	99.3
Replacement zones																
IR20	Shallow	12.6	50.8	66.4	17.5	33.3	3.0	10.8	1.1	0.21	0.52	2.7	0.36	0.49	30.5	100.5
IN2	Very shallow	12.3	51.4	66.8	18.3	33.1	3.1	10.8	1.1	0.02	0.36	3.3	0.60	0.22	30.4	101.3
IM3	Shallow	14.4	47.9	65.3	16.0	31.9	3.1	11.2	1.6	0.36	1.22	3.7	0.43	0.65	30.9	101.1
IM4P	Shallow-pegmatite	18.4	40.8	62.5	12.0	28.8	3.3	12.3	3.1	0.85	2.15	4.4	0.32	0.97	30.9	99.4
IM1	Medium-deformed	14.9	46.9	64.9	15.3	31.6	3.1	11.3	1.7	0.50	1.42	3.7	0.37	0.61	30.6	100.3
RMC3	Deep?	16.6	45.6	65.2	15.1	30.5	3.1	11.7	1.9	0.70	2.25	3.1	0.18	0.71	31.1	100.4
IM5	Xenolith in AW	17.5	40.3	60.8	12.0	28.2	3.0	11.7	2.7	0.80	2.29	5.3	0.34	1.12	30.4	98.2
IR1	Deep	19.2	38.4	60.8	11.2	27.2	3.2	13.1	2.8	0.87	2.44	6.3	0.70	1.08	29.5	98.9
OS8C	Deep	14.6	44.6	62.1	14.5	30.2	2.9	10.3	1.6	0.49	2.11	6.3	1.22	0.55	29.0	99.2

Ca. Apatite ($CaPO_4$) inclusions are abundant in most of these grains, and the most plausible explanation for this deviation is that analyses performed in automated mode were slightly off their intended locations and overlapped inclusions, thus increasing the amount of Ca in the analysis.

Magmatic zones from most samples cluster around 0.02–0.06 atoms/formula Ca and 0–0.03 atoms/formula Si (Fig. 6a). Replacement zones from the most highly modified samples tend to have higher Si than magmatic zones but no enrichment in Ca (most samples show a depletion). These zones are high in Th as well as Si (Fig. 6c), indicating a large huttonite component. Replacement zones from less modified samples show little enrichment in Si and Th. However, they tend to be depleted in Ca relative to magmatic zones and have Si/Th closer to unity, suggesting that huttonite substitution assumes greater importance at the expense of brabantite.

Table 2 shows average chemical compositions for primary and replacement zones. Replacement zones from samples deeper in the pluton are higher in Th and Si than those from shallow samples. Sample IM1, which has a relatively low-*T* ductile fabric and was only moderately deep, has replacement zones that share compositional characteristics with those from shallow samples. Replacement zones from sample RMC3 are also compositionally similar to shallow-level replacement zones, despite the sample's apparent depth; structural evidence and its relatively low-*T* fabric suggest that this area may have been faulted downward to its present position along a normal-sense shear zone (Bachl, 1997; J.E. Faulds, personal communication).

Average elemental compositions of the different zone types are shown in Table 3. Among the patchy zones, Th and Si increase with increasing BSE brightness while Ca and LREE decrease. Though veins tend to be generally lower in Th than patchy zones, they are brighter and higher in Si and Th than surrounding homogeneous or oscillatory material in the same grain. Higher Si indicates that more of the Th present in veins is in the form of huttonite, which has a higher mean atomic number and is therefore brighter than monazite. Brabantite, in contrast, has a similar atomic number and therefore Th in brabantite substitution has little effect on brightness. Very small, particularly bright regions in monazites may be extremely huttonite-rich zones or thorite ($ThSiO_4$) inclusions rather than monazite. Though they are too small to permit good analyses, they are richer in Th than all other types of monazite zones. Oscillatory zones are lower in Th and Si and higher in Ca than most replacement zones.

REE distribution does not show a distinct fractionation between primary and replacement zones (Fig. 7). LREE/HREE ratios do not differ systematically in magmatic and replacement zones, and they do not vary as a function of depth or deformation or proximity to Miocene plutons. For the most part, the patterns permit local sources (sample scale?) for the REE in replacement zones. In the two deepest samples, IR1 and OS8C (Fig. 7c), compositions of replacement zones appear to be distinctly different from magmatic zones, but the apparent fractionation in the two samples is opposite in sense: most OS8C replacement zones are enriched in LREE (La) and depleted in middle REE (Sm), while IR1 replacement zones are generally depleted in LREE.

5. Discussion

BSE imaging of monazite from the Ireteba pluton reveals zones of differing brightness (= composition) that replaced magmatic monazite, overprinting or obliterating the primary magmatic zoning. Boundaries between zones are sharp, and replacement zones are present throughout grains and show no spatial correlation to grain surfaces, indicating that bulk diffusion was not the mechanism that modified composition. Replacement in the interior of crystals entailed little or no volume change, though crystal surfaces were corroded and in some cases secondary overgrowths were added. The cause(s) of replacement is not obvious. Except in sample IM5, from a xenolith in the Aztec Wash pluton, samples appear to have petrographically undergone limited alteration (minor chlorite replacement of biotite, no epidote or calcite, little sericitization of feldspar). There is a correlation between deformation and degree of monazite replacement, yet some deformed samples have little replacement. Replacement cannot be simply attributed to processes that have visibly modified the

Table 3
Average elemental composition of zoning types (EMP). All compositions in oxide wt.%

Zone type	HREE	LREE	REE	La_2O_3	Ce_2O_3	Pr_2O_3	Nd_2O_3	Sm_2O_3	Dy_2O_3	Y_2O_3	ThO_2	SiO_2	CaO	P_2O_5	Total
Bright	15.8	43.4	62.3	13.7	29.7	3.2	11.6	2.3	0.46	1.3	7.0	1.36	0.56	29.2	100.5
Convoluted	14.1	45.0	62.0	14.7	30.3	2.9	10.0	1.4	0.46	2.2	6.4	1.35	0.48	28.8	99.2
Patchy-light	17.5	41.8	62.4	12.7	29.1	3.1	12.4	2.5	0.73	1.9	5.4	0.65	0.78	29.9	99.5
Patchy-medium	17.1	42.7	62.9	13.3	29.4	3.1	11.9	2.3	0.75	2.1	4.6	0.37	0.90	30.3	99.4
Patchy-dark	17.2	42.9	63.2	13.5	29.4	3.1	11.8	2.3	0.76	2.3	3.8	0.14	1.03	30.8	99.3
Rim	14.1	47.1	64.2	15.7	31.4	3.0	11.1	1.5	0.35	1.2	3.8	0.35	0.90	30.7	100.0
Recrystallized core	14.3	47.7	65.1	16.0	31.7	3.1	11.3	1.6	0.32	1.1	3.5	0.29	0.70	30.4	100.1
Oscillatory	14.6	46.9	64.5	15.7	31.2	3.0	11.0	1.6	0.46	1.5	3.4	0.17	0.96	30.8	99.9
Vein	13.4	49.7	66.1	16.9	32.8	3.1	11.1	1.4	0.25	0.7	3.3	0.47	0.38	30.4	100.8
Inherited cores	12.3	50.4	65.6	17.7	32.7	2.9	10.7	1.0	0.21	0.4	2.5	0.35	1.16	30.1	99.7
Homogeneous	12.7	48.9	64.5	16.8	32.1	2.9	10.6	1.1	0.28	0.7	2.5	0.32	1.33	29.7	98.4

host rock. The following discussion examines the conditions under which monazite was replaced and the variations in conditions associated with different types of replacement zones.

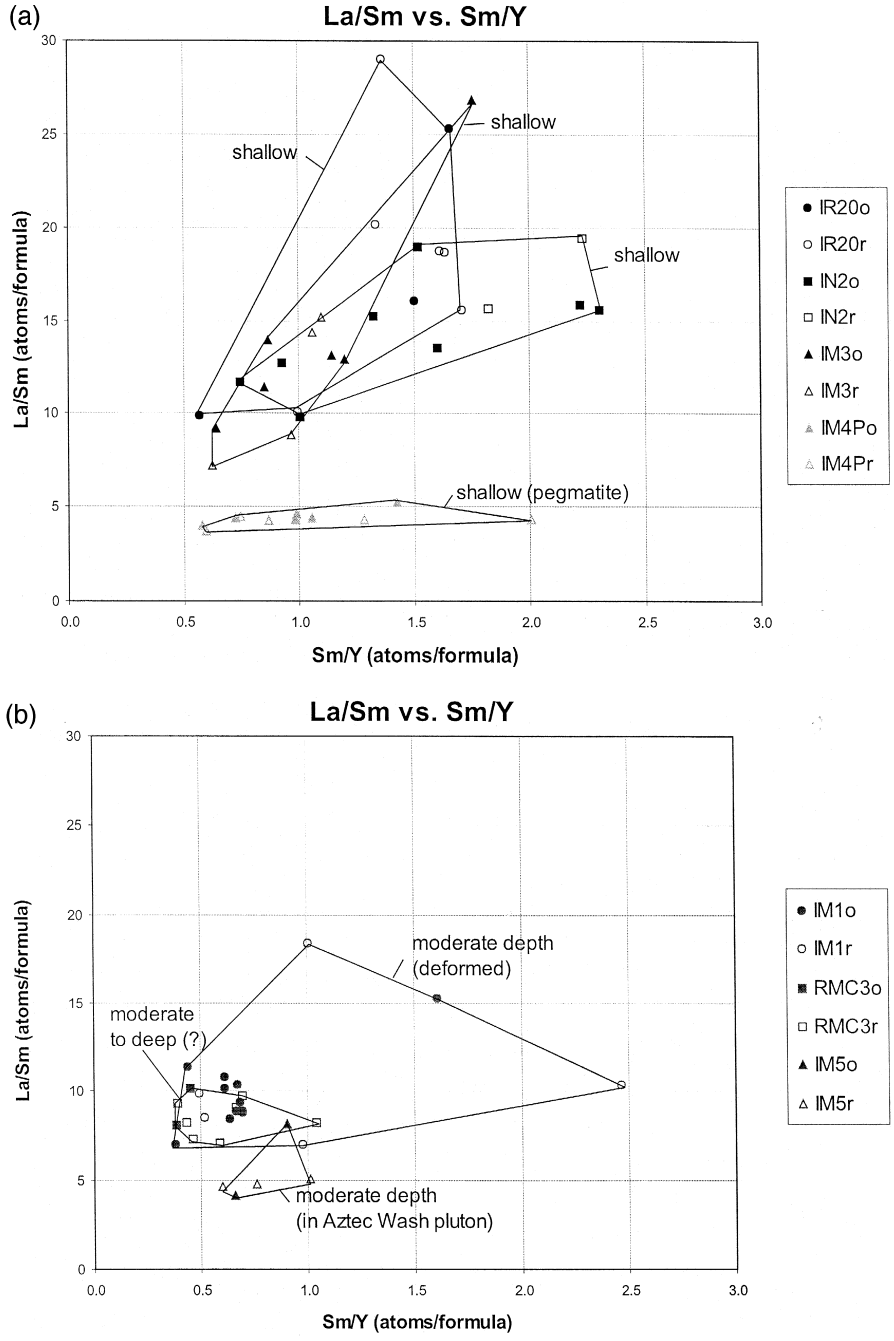

Fig. 7. (a,b,c) Concentrations of selected REE per formula. Analyses of original magmatic (o; filled symbols) and replacement (r; open symbols) zones, broken down by sample.

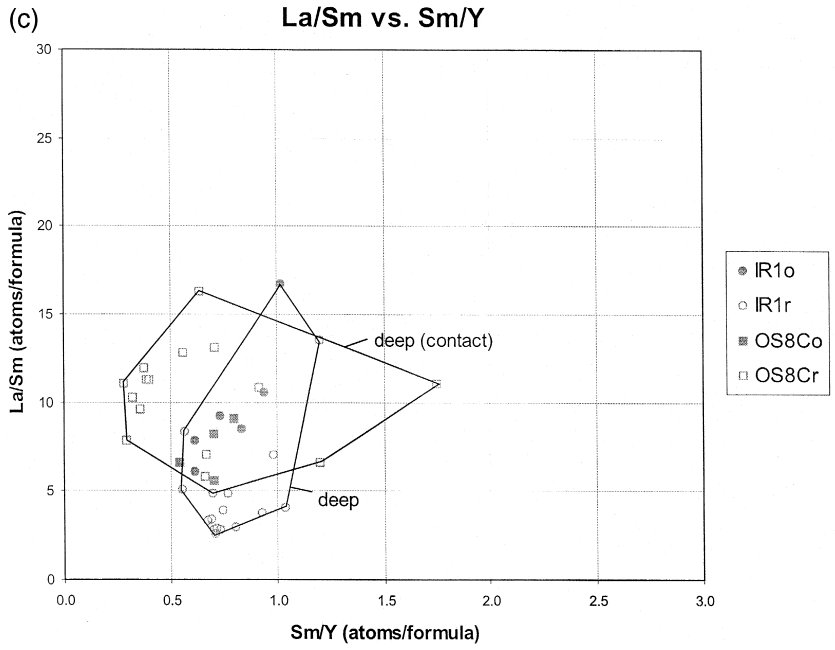

Fig. 7 (*continued*).

5.1. Temperature of replacement and Th–Pb resetting

Monazite is commonly interpreted to retain Pb up to 700–750°C. However, this interpretation assumes Pb loss by bulk diffusion and not resetting by recrystallization. $^{40}Ar/^{39}Ar$ analyses of muscovite and biotite constrain temperatures experienced by the Ireteba pluton in the mid-Miocene (M.T. Heizler, 1998, unpublished data). Based on these constraints, it appears that resetting of monazite took place far below its closure temperature. Muscovite from the west (shallow) side of the pluton yields erratic spectra that reflect only modest mid-Cenozoic Ar loss, whereas biotite was largely degassed during the Miocene. This area, includes samples IM3, IM4, and IR20. Farther to the east, both muscovite and biotite yield 15–16 Ma ages. These data suggest that shallow parts of the pluton were cooler than 350–400°C at ~16 Ma while deeper regions were hotter than ~400°C. Because samples IM3 and IR20 have zones that we interpret to have formed during the Miocene, we infer that monazite was reset by replacement at temperatures below 350–400°C.

Samples IM1, IM2, IR1 and OS8C are from increasingly deeper, warmer areas of the pluton. This temperature distribution is consistent with deformation textures that suggest incipient ductility of quartz in the west-central part of the pluton and feldspar ductility toward the eastern side. Temperatures very close to the Aztec Wash and Searchlight plutons (samples IN2, IM5, OS8C and RMC3) were presumably significantly elevated. Among these samples, monazite replacement and mid-Miocene ages are most extensive in IR1 and OS8C, which are both deep and close to the Searchlight pluton. (There are no reliable age data from the single monazite grain from IM5, the xenolith in the Aztec Wash pluton.) Although temperatures in the deeper areas exceeded 400°C, it is highly unlikely that they exceeded 700°C for an appreciable period of time in the Cenozoic.

5.2. Depth and deformation

Deformation within the Ireteba pluton increases with depth, and monazite replacement roughly correlates with both, but deformation alone does not appear to have instigated replacement. For example,

strongly lineated sample IM1 has euhedral monazite that underwent limited replacement. Deformed samples that were deeper than IM1 (~10 km at ~16 Ma) do have extensive replacement.

5.3. Proximity to Miocene plutons

Samples IR1 and OS8C, which were near the Miocene Searchlight pluton, were also deep in the Miocene (> 10 km). These samples have the highest degree of monazite replacement and the replacement zones tend to be enriched in Th and Si relative to magmatic zones. The compositional differences between magmatic and replacement zones may be due to the influence of fluids interacting with the host rock during recrystallization. The most likely sources for such fluids are the Miocene plutons. We note that if fluid influx was the cause of replacement, then the influence of these fluids must have been highly selective because other minerals were not appreciably altered.

The paucity of secondary monazite from shallow sample IN2, collected ~200 m from the roof of the Aztec Wash pluton, suggests that proximity to Miocene plutons is not a sufficient condition for replacement. Replacement zones from this sample are not substantially enriched in Th and Si relative to magmatic zones. Sample IM5, from a large xenolith of Ireteba granite in the Aztec Wash pluton, has extremely sparse monazite; most primary grains were probably replaced by secondary allanite, thorite, and sphene, which are absent in other samples.

Proximity to Miocene plutons alone did not guarantee extensive replacement, as indicated by relatively unaltered monazite near Aztec Wash contacts. Perhaps depth and/or the abundance or composition of expelled fluid were factors leading to more extensive replacement near the Searchlight pluton contact.

5.4. Conditions affecting the nature of replacement zones

Veins formed in monazite from shallow parts of the pluton, regardless of proximity to Miocene plutons. Formation of veins therefore must not require that the host rock be subjected to intense heating. On the contrary, monazite from samples that were heated significantly (above ~400°C) during Miocene pluton intrusion show very little veining, and the sample from the Ireteba–Searchlight contact shows none at all. This relationship may suggest either that veins were a precursor to the more extensive replacement zoning displayed in samples exposed to higher temperatures or that brittle fracturing of monazite was an important factor in controlling replacement at lower temperature but not in deeper rocks.

Patchy zoning formed in monazite from all parts of the pluton but was least extensive in shallow samples and most pervasive in deep samples. Its formation during the Miocene in shallow rocks suggests that patchy zoning does not require temperatures above 350–400°C, but its correlation with depth suggests that it is facilitated by high T.

Convolute zoning formed only in the sample from the Ireteba–Searchlight contact. This type of zoning, like well-developed patchy zoning, probably formed during exposure of the rock to heat and hydrothermal fluids from the Searchlight pluton. Either depth or characteristics particular to fluids emanating from the Searchlight pluton (but not from the Aztec Wash pluton) resulted in convolute zoning in addition to patchy zoning.

The origin of the sector zoning in samples IR20 and OS8C is unknown because these zones were not dated. Such zoning in other minerals is generally considered to be a magmatic texture. However, based on its most common occurrence in OS8C (from the Searchlight Ireteba contact), where monazite is quite thoroughly replaced, it may be a secondary feature.

Irregular rims formed in shallow to moderately deep, deformed and undeformed samples. Because their ages are primarily ~60 Ma, they may have formed during the initial crystallization or during an event that occurred shortly thereafter. The conditions responsible for their formation are unknown.

5.5. Episodes of monazite replacement in the Ireteba pluton

Our data require one and suggest a second replacement episode since crystallization of the Ireteba pluton at 64 Ma. The dominant event coincides with the intrusion of Miocene plutons and extension at about 16 Ma. A few patchy and most irregular rim

zones yield older ages (59–65 Ma), which may indicate that some replacement occurred during or immediately after crystallization of the pluton, possibly in response to fluids circulating in the cooling rock.

5.6. Implications for geochronology

This work supports recent studies that indicate that monazite is susceptible to replacement and that interpretation of radiometric ages of monazite is therefore much less straightforward than commonly assumed (e.g. DeWolf et al., 1993; Hawkins and Bowring, 1997; Zhu et al., 1997; Crowley and Ghent, 1999; Vavra and Schaltegger, 1999). In order to use monazite geochronology effectively, it is important to know whether replacement has occurred. Monazite replacement may be a common phenomenon. SEM imaging of monazite surface texture may give an indication of the degree of replacement in the grain, but BSE imaging of internal zones in polished grains gives the most obvious evidence of replacement. With knowledge of the internal texture of monazite grains, more information can be gleaned about events that affected them. Previous geochronological studies may be enhanced by examining zoning, and future studies may yield more detailed conclusions. Further work on this subject will better define the geochemical and thermal conditions that result in monazite replacement.

6. Summary

6.1. Conclusions

1. The Ireteba pluton experienced one episode of monazite replacement at ~16 Ma, and possibly an earlier episode shortly after crystallization of the magma.
2. Monazite from samples from deep levels that are close to the 16 Ma Searchlight pluton are most highly replaced.
3. Some monazite recrystallized at low temperatures ($< 400°C$).
4. Even in rocks that are undeformed, distant from younger intrusions, and apparently unaltered, monazite was partly replaced.
5. Surface alteration of monazite correlates with internal modification.
6. Younger ages are due to recrystallization, not diffusive Pb loss.
7. Hydrothermal fluids may have caused or enhanced replacement.
8. Deformation may have increased the extent of replacement in monazite subjected to hydrothermal fluids.
9. Increasing depth may have enhanced replacement processes.

6.2. Implications

1. In order to use monazite geochronology effectively, it is important to know whether replacement occurred.
2. There may be no macroscopic way to identify rocks in which monazite has been replaced; examination of monazite surface texture may provide clues, but BSE imaging of internal structures is most effective and may be necessary.
3. Monazite dating is, in many cases, more complex than originally assumed and may require imaging of internal structures and spot (IMP) analysis.
4. Using these techniques, monazite may provide additional information about events that affected the host rocks.
5. Previous studies using conventional dating of monazite may be enhanced by reexamining monazite in light of new observations.
6. Further work on this subject should include definition of the geochemical and thermal conditions required for monazite replacement.

Acknowledgements

We thank Dave Wark and Kyra Banks, who provided guidance for electron microprobe analysis at Rensselaer Polytechnic Institute; Sam Vinson, who discussed many aspects of the research as it progressed and helped with many laboratory procedures; and Jim Faulds, who contributed invaluable insights to the field aspects of this study. Matt Heizler shared

unpublished data that were invaluable in interpreting the thermal history of the area. Discussions with Peter Gromet, John Hanchar, Bruce Watson and Dave Wark provided useful ideas and perspectives. Jim Crowley and David Hawkins provided thorough and thoughtful reviews that were a great help in clarifying the paper. This research was supported by NSF grants EAR 9506651, 9628380, and 9873626. The UCLA ion microprobe laboratory is partially supported by a grant from the NSF Instrumentation and Facilities Program.

References

Bachl, C.A., 1997. The Searchlight pluton: an example of wholesale magmatic reconstruction of the upper crust during continental extension. Master's thesis, Vanderbilt University, Nashville, TN.

Carl, B.S., Miller, C.F., Foster, D.A., 1991. Western Old Woman Mountains shear zone: evidence for late ductile extension in the Cordilleran orogenic belt. Geology 19, 893–896.

Copeland, P., Parrish, R.R., Harrison, T.M., 1988. Identification of inherited Pb in monazite and its implications for U–Pb systematics. Nature 333, 760–763.

Crowley, J.L., Ghent, E.D., 1999. An electron microprobe study of the U–Th–Pb systematics of metamorphosed monazite: the role of Pb diffusion versus overgrowth and recrystallization. Chem. Geol. 157, 285–302.

D'Andrea, J.L., 1998. Geology and petrogenesis of the Ireteba Pluton: implications for the generation of peraluminous granites. Master's thesis, Vanderbilt University, Nashville, TN.

Deino, A., Potts, R., 1992. Age-probability spectra for examination of single-crystal $^{40}Ar/^{39}Ar$ dating results; examples from Olorgasailie, southern Kenya Rift. In: Westgate, J.A., Walter, R.C., Naeser, N. (Eds.), Tephrochronology: stratigraphic applications of tephra. Quaternary International Meeting, Yellowstone National Park, USA, pp. 47–53.

DeWolf, C.P., Belshaw, N.S., O'Nions, R., Keith, A., 1993. Metamorphic history from micron-scale $^{207}Pb/^{206}Pb$ chronometry of Archean monazite. Earth Planet. Sci. Lett. 120, 207–220.

Falkner, C.M., Miller, C.F., Wooden, J.L., Heizler, M.T., 1995. Petrogenesis and tectonic significance of the calc–alkaline, bimodal Aztec Wash pluton, Eldorado Mountains, Colorado River extensional corridor. J. Geophys. Res. 100, 10453–10476.

Faulds, J.E., Geissman, J.W., Mawer, C.K., 1990. Structural development of a major extensional accommodation zone in the Basin and Range Province, northwestern Arizona and southern Nevada: implications for kinematic models of continental extension. Geol. Soc. Am. Mem. 176, 37–76.

Fitzsimmons, I.C.W., Kinny, P.D., Harley, S.L., 1997. Two stages of zircon and monazite growth in anatectic leucogneiss; SHRIMP constraints on the duration and intensity of Pan-African metamorphism in Prydz Bay, East Antarctica. Terra Nova 9, 47–51.

Gans, P.B., Landau, B., 1993. Initially vertical normal faults and runaway block rotations in the basin and range province: some geological and mechanical observations. Geol. Soc. Am., Abstr. Prog. 25, 40.

Hanchar, J.M., Miller, C.F., 1993. Zircon zonation patterns as revealed by cathodo-luminescence and backscattered electron images: implications for interpretation of complex crustal histories. Chem. Geol. 110, 1–14.

Harrison, T.M., McKeegan, K.D., Lefort, P., 1995. Detection of inherited monazite in the Manaslu leucogranite by $^{208}Pb/^{232}Th$ ion microprobe dating: crystallization age and tectonic significance. Earth Planet. Sci. Lett. 133, 271–282.

Hawkins, D.P., Bowring, S.A., 1997. U–Pb systematics of monazite and xenotime: case studies from the Paleoproterozoic of the Grand Canyon, Arizona. Contrib. Mineral. Petrol. 127, 87–103.

Hawkins, D.P., Bowring, S.A., 1999. U–Pb monazite, xenotime and titanite geochronological constraints on the prograde to post-peak metamorphic thermal history of Paleoproterozoic migmatites from the Grand Canyon, Arizona. Contrib. Mineral. Petrol. 134, 150–169.

Heaman, L., Parrish, R., 1991. U–Pb geochronology of accessory minerals. In: Heaman, L., Ludden, J.N. (Eds.), Applications of radiogenic isotope systems to problems in geology. Min. Assoc. Canada Handbook, pp. 59–102.

Kingsbury, J.A., Miller, C.F., Wooden, J.L., Harrison, T.M., 1993. Monazite paragenesis and U–Pb systematics in rocks of the eastern Mojave Desert, California: implications for thermochronometry. Chem. Geol. 110, 147–168.

Kroener, A., Williams, I.S., 1993. Age of metamorphism in the high-grade rocks of Sri Lanka. J. Geol. 101, 513–521.

Miller, C.F., D'Andrea, J.L., Ayers, J.C., Coath, C.D., Harrison, T.M., 1997. BSE imaging and ion probe geochronology of zircon and monazite from plutons of the Eldorado and Newberry Mountains, Nevada: age, inheritance, and subsolidus modification. EOS 78, F783.

Parrish, R.R., 1990. U–Pb dating of monazite and its application to geological problems. Can. J. Earth Sci. 27, 1431–1450.

Patrick, D.W., Miller, C.F., 1997. Processes in a composite, recharging magma chamber: evidence from magmatic structures in the Aztec Wash pluton, Nevada. Proc. of the 30th Intl. Geol. Congr. (Research Volume), 121–135.

Poitrasson, F., Chenery, S., Bland, D.J., 1996. Contrasted monazite hydrothermal alteration mechanisms and their geochemical implications. Earth Planet. Sci. Lett. 145, 79–96.

Schärer, U., 1984. The effect of initial ^{230}Th disequilibrium on young U–Pb ages: the Makalu case, Himalaya. Earth Planet. Sci. Lett. 67, 611–619.

Shaw, M.L., Faulds, J.E., Miller, C.F., 1995. Tectono-magmatic evolution of the southern Eldorado Mountains, Nevada: a glimpse into the progressive development of a major normal fault zone. Geol. Soc. Am., Abstr. Prog. 27 (6), A120.

Smith, H.A., Barreiro, B., 1990. Monazite U–Pb dating of stauro-

lite grade metamorphism in pelitic schists. Contrib. Mineral. Petrol. 105, 602–615.

Smith, H.A., Giletti, B.J., 1997. Lead diffusion in monazite. Geochim. Cosmochim. Acta 61, 1047–1055.

Suzuki, K., Adachi, M., Kajizuka, I., 1994. Electron microprobe observations of Pb diffusion in metamorphosed detrital monazites. Earth Planet. Sci. Lett. 128, 391–405.

Vavra, G., Schaltegger, U., 1999. Post-granulite facies monazite growth and rejuvenation during Permian to Lower Jurassic thermal and fluid events in the Ivrea Zone (Southern Alps). Contrib. Mineral. Petrol. 134, 405–414.

Wark, D.A., Miller, C.F., 1993. Accessory mineral behavior during differentiation of a granite suite: monazite, xenotime and zircon in the Sweetwater Wash pluton. Chem. Geol. 110, 49–67.

Zhu, X.K., O'Nions, R.K., Belshaw, N.S., Gibb, A.J., 1997. Significance of in situ SIMS chronometry of zoned monazite from the Lewisian granulites, northwest Scotland. Chem. Geol. 135, 35–53.

Zhu, X.K., O'Nions, R.K., 1999. Zonation of monazite in metamorphic rocks: a case study from the Lewisian terrain. Earth Planet. Sci. Lett. 171, 209–220.